

Optomechanical Dirac Physics

M. Schmidt,¹ V. Peano,¹ and F. Marquardt^{1,2}

¹University of Erlangen-Nürnberg, Staudtstr. 7, Institute for Theoretical Physics, D-91058 Erlangen, Germany
²Max Planck Institute for the Science of Light, Günther-Scharowsky-Straße 1/Bau 24, D-91058 Erlangen, Germany

Recent progress in optomechanical systems may soon allow the realization of optomechanical arrays, i.e. periodic arrangements of interacting optical and vibrational modes. We show that photons and phonons on a honeycomb lattice will produce an optically tunable Dirac-type band structure. Transport in such a system can exhibit transmission through an optically created barrier, similar to Klein tunneling, but with interconversion between light and sound. In addition, edge states at the sample boundaries are dispersive and enable controlled propagation of photon-phonon polaritons.

PACS numbers: 42.50.Wk, 42.65.Sf

Rapid progress is being made in the field of optomechanics, which studies the interaction of light with nanomechanical motion (for a recent review, see [1]). Most current achievements are based on a single vibrational mode coupled to a single optical mode (i.e. a single “optomechanical cell”). A logical next step is to couple many such modes, providing new functionality and generating new physical phenomena. First steps have been taken using setups with a few modes (e.g. for synchronization [2, 3], wavelength conversion [4, 5], phonon lasing [6], or cooling [7]). Going beyond this, we can envisage a periodic arrangement of cells. In that case we will speak of an “optomechanical array”. Optomechanical arrays might be realized on a number of experimental platforms: Microdiscs [2, 8] and microtoroids [9, 10] could be coupled via evanescent optical fields [2]. Superconducting on-chip microwave cavity arrays (of the type discussed in [11]) could be combined with nanobeams [12] or membranes [13]. Currently the most promising platform are optomechanical crystals, i.e. photonic crystals engineered to contain localized vibrational and optical modes. Single-mode optomechanical systems based on that concept have been demonstrated experimentally, with very favorable parameters [14–18]. Ab-initio simulations indicate the feasibility of arrays [19–21]. Given these developments it seems that optomechanical arrays are on the verge of realization. The existing theoretical work on optomechanical arrays deals with slow light [22], synchronization [20, 21, 23], quantum information processing [24] and quantum many-body physics [21, 25–28] and photon transport [29]. In this letter, we go beyond these works and illustrate the possibilities offered by engineering non-trivial optomechanical band structures of photons and phonons in such arrays. Specifically, we will investigate an array with a honeycomb geometry. This lattice is the basis for modeling electrons in graphene [30], but it has recently also been studied for photonic crystals [31, 32], exciton-photon polaritons [33] and other systems [32]. It is the simplest lattice with a band structure showing singular and robust features called Dirac cones, mimicking

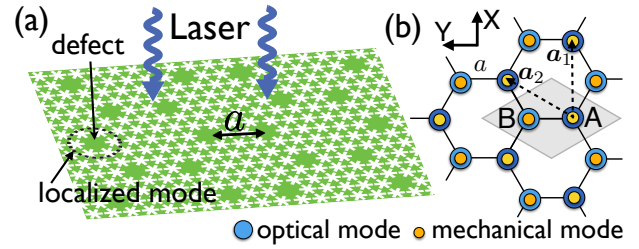


Figure 1: (a) Setup: Thin slabs of free-standing dielectric (green) with periodically etched holes (white), so-called optomechanical crystals [14–17, 34], are known to give rise to an optomechanical interaction of localized optical ($\sim 10^2$ THz) and vibrational modes (\sim GHz) at engineered defects. The interaction is controlled by a driving laser. When extended to an array, the modes of nearby defect sites will be connected via phonon and photon tunneling. (b) We consider defects arranged in a honeycomb superlattice.

the dispersion of relativistic massless particles. As we will be interested in the long-wavelength properties of the structure, on scales much larger than the lattice spacing, we may call this an “optomechanical metamaterial”. Tunability would be the biggest advantage of optomechanical metamaterials, rivaling that of optical lattices: The band structure is easily tunable by the laser drive (intensity, frequency, phases). Moreover, it can be observed by monitoring the emitted light. Using spatial intensity profiles for driving, one can even engineer arbitrary potentials and hence local changes in the band structure. We predict that these features could be used to observe photon-phonon Dirac polaritons, an optomechanical Klein tunneling effect, and edge state transport.

Model - We consider a 2D honeycomb lattice of identical optomechanical cells, driven uniformly by a laser (frequency ω_L). Each cell supports a pair of co-localized mechanical (eigenfrequency Ω) and optical (eigenfrequency ω_{cav}) modes interacting via radiation pressure. This geometry could be implemented based on optomechanical crystals, see Figure 1, but also in other physical realiza-

tions such as arrays of microdisks, microtoroids, or superconducting cavities. We adopt the standard approach of linearizing the dynamics around the steady-state classical solution and performing the rotating wave approximation, valid for red detuned ($\Delta = \omega_L - \omega_{\text{cav}} < 0$) moderate driving [1]. In a frame rotating with the drive, the linearized Hamiltonian reads

$$\hat{H}/\hbar = \sum_j \Omega \hat{b}_j^\dagger \hat{b}_j - \Delta \hat{a}_j^\dagger \hat{a}_j - g_j (\hat{b}_j^\dagger \hat{a}_j + \hat{a}_j^\dagger \hat{b}_j) + \hat{H}_{\text{hop}}. \quad (1)$$

This Hamiltonian describes the non-equilibrium physics of the array of phonon modes (annihilation operator \hat{b}_j) and photon modes (\hat{a}_j), interacting via the linearized optomechanical interaction of strength g_j . The term $\hat{H}_{\text{hop}} = -\sum (J_{ij} \hat{a}_i^\dagger \hat{a}_j + K_{ij} \hat{b}_i^\dagger \hat{b}_j)$ describes the tunneling of photons and phonons between neighboring sites i and j with amplitudes J_{ij} and K_{ij} , respectively [19–21]. Here, $j = [m, n, \sigma]$ is a multi-index, where m, n indicate the unit cell, which contains two optomechanical cells on sublattices A/B (denoted by $\sigma = \pm 1$).

The interaction strength is $g_j = g_0 \alpha_j$, where g_0 is the bare optomechanical coupling, i.e. the shift of the local optical resonance by a mechanical zero-point displacement, and α_j is the local complex light field amplitude, proportional to the laser amplitude [1]. For completeness, we mention that the operators \hat{a}_j and \hat{b}_j in Eq. (1) are assumed shifted, as usual [1], by α_j and by the radiation-pressure-induced mechanical displacement β_j , respectively. The detuning $\Delta = \omega_L - \omega_{\text{cav}}$ incorporates a small shift in ω_{cav} due to the static mechanical displacement.

The eigenfrequencies of Hamiltonian (1) form the optomechanical band structure, shown in Fig. 2 (a,b) for realistic parameters and a translationally invariant system ($g_j = g$). It comprises four polariton bands, constructed out of the original two photon and two phonon bands, giving rise to photon-phonon polariton Dirac cones.

A weak additional probe laser can inject excitations at arbitrary frequency. It can be spatially resolved (via tapered fiber) or momentum-resolved (extended beam). Even without the probe, the momentum-resolved band structure is visible in the emitted far-field radiation in the form of Raman-scattered laser-drive photons, see Fig. 2 (d,e). We incorporate dissipation and noise via the standard input/output theory [1], taking into account the photon (phonon) decay rate κ (Γ) and the thermal phonon number \bar{n} , see Supplemental Material. We emphasize that the band structure (and transport) could be observed in this manner even at room temperature.

The emergence of the Dirac cones at the Dirac points \mathbf{K} and \mathbf{K}' follows from the symmetries of the honeycomb lattice [35]. Without the drive ($g_j = 0$), the standard scenario for honeycomb lattices applies to photons and phonons separately: Excitations can be on sublattice A or B, corresponding to a binary degree of freedom, $\sigma_z = \sigma = \pm 1$. Diagonalizing the Hamiltonian using

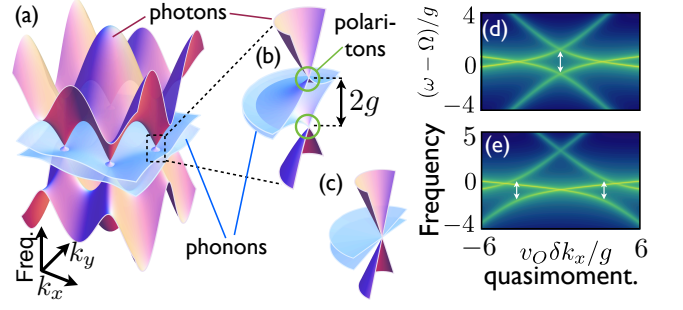


Figure 2: (a) Band structure of an optomechanical honeycomb array, featuring fast photons and slow phonons that interact optomechanically. Detuning the driving laser will shift the photon band up and down. Here, the photon and phonon Dirac points are chosen resonant, thus photon-phonon polariton Dirac cones emerge in their vicinity for $g \neq 0$, see the close-up in (b). (c) Without optomechanical interaction, $g = 0$, photon and phonon cones would simply intersect. (d) A cut through the spectrum $S(\mathbf{k}, \omega)$ of the light scattered by the setup reproduces the band structure, in the presence of dissipation. (e) Detuned case: Avoided crossing (arrows) between bands with equal helicity, see main text. [Parameters: $v_M = v_O/10$, $g = J/10$, $\Delta = -\Omega$ (a-d), $\Delta = -\Omega - 3g$ (e), (d,e): $J = \Omega/3$, $\kappa = J/100$, $\Gamma = \kappa/10$, $\bar{n} = 5000$]

a plane wave ansatz, one recovers a 2×2 Hamiltonian for every wave vector \mathbf{k} . Close to a symmetry point, this reduces to the Dirac Hamiltonian for $2D$ relativistic massless particles. Around \mathbf{K} , it has the form $\hbar v \hat{\sigma} \cdot \delta \mathbf{k}$, where $\delta \mathbf{k} = \mathbf{k} - \mathbf{K}$ and $\hat{\sigma}$ is the vector of Pauli matrices $\hat{\sigma}_{x,y}$. The photon velocity at the Dirac point, v_O , will be generally significantly larger than the mechanical one, v_M , see Fig. 2(c). For nearest-neighbor hopping amplitudes J (photons) and K (phonons), we find $v_O = 3aJ/2$, $v_M = 3aK/2$.

We now consider the interacting case ($g \neq 0$), turning the Hamiltonian (1) into its first-quantized counterpart in momentum space and expanding it around a symmetry point. The particle type can now be encoded in a second binary degree of freedom, $\tau_z = \tau = \pm 1$ for photons/phonons (with Pauli matrices $\hat{\tau}_{x,z}$). We find the optomechanical Dirac Hamiltonian:

$$\hat{H}_D/\hbar = \delta\omega \hat{\tau}_z/2 + (\bar{v} + \delta v \hat{\tau}_z/2) \hat{\sigma} \cdot \delta \mathbf{k} - g \hat{\tau}_x + \bar{\omega}. \quad (2)$$

This Hamiltonian describes the mixing of two excitations of very different physical origin, with properties that are easily tunable. The terms describe, in this order, an offset between photon and phonon bands, the Dirac part, and the optomechanical interaction (plus a constant offset). Here we defined $\bar{v} = (v_O + v_M)/2$, $\delta v = v_O - v_M$, $\bar{\omega} = (\Omega - \Delta)/2$, and $\delta\omega = -\Delta - \Omega$. The interaction g is tunable in-situ via the drive laser intensity (in contrast, e.g., to bilayer graphene systems). Photon-phonon Dirac polaritons feature a dispersive spectrum

$$\omega_{\tau,\sigma}(\mathbf{k}) = \bar{\omega} - \sigma \bar{v} |\delta \mathbf{k}| + \tau \sqrt{g^2 + (\delta\omega - \sigma \delta v |\delta \mathbf{k}|)^2}/4, \quad (3)$$

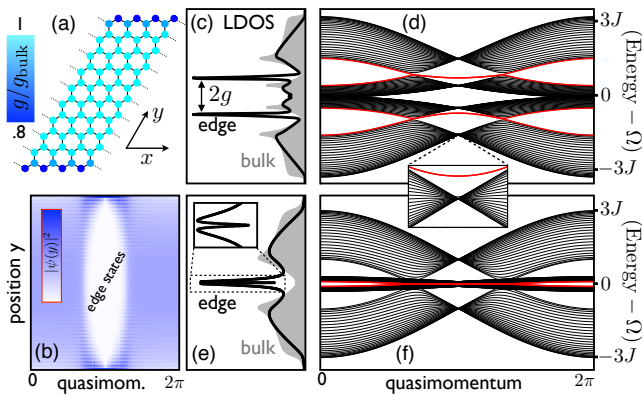


Figure 3: Polaron edge states of a semi-infinite optomechanical strip (zigzag edge) differ from usual edge states in honeycomb lattices. (a) Optomechanical interaction strength $g(y)$ of a homogeneously driven strip. (b) Wavefunction of the upper edge state band. (c) Local DOS (experimentally accessible via a probe laser) in the bulk (gray) and at the edge (black) reveals the existence of edge states (here for $g \gg \kappa$). (d) Corresponding band structure (real part of eigenfrequencies), indicating the dispersive nature of the edge states (in red). (e) For $g \ll \kappa$, a sharp dip is observable, due to optomechanically induced transparency (width $\sim \Gamma$). (f) Band structure for $g \ll \kappa$. [Parameters: $J = \Omega/6$, $K = 0.1J$, $g_{\text{bulk}} = 0.007\Omega$ (e,f), $g_{\text{bulk}} = 0.15$ (else), $-\Delta = \Omega$, $\kappa = 0.04\Omega$ (e,f), $\kappa = 0.01\Omega$ (else), $\Gamma = 0.001\Omega$;]

i. e. the velocity is momentum-dependent and varies on the momentum scale g/Ja , well within the range of validity of Eq. (2), $|\delta\vec{k}| \ll a^{-1}$. This effect comes from the mixing of two Dirac excitations with different velocities.

At the Dirac points, the band structure comprises two pairs of cones split by $\sqrt{\delta\omega^2 + 4g^2}$. Sweeping the laser detuning $\delta\omega$ from positive to negative values, the upper cones evolve from purely optical (velocity v_O), over polaritonic (slope $\bar{v} = (v_O + v_M)/2$) to purely mechanical (velocity v_M). Since the helicity, $\hat{\sigma} \cdot \delta\mathbf{k}/|\delta\mathbf{k}|$, is conserved, bands of equal helicity feature avoided crossings, while bands of different helicity cross, see Fig. 2(d,e).

Edge states - The physics of edge states is significantly modified by inhomogeneous optomechanical couplings that can be tailored via the laser intensity but also naturally occur in a finite system under uniform drive. There, the coupling is smaller at the edges than in the bulk, see Fig. 3(a). In an infinite strip with zigzag edges this leads to a band of polariton edge modes with tunable velocity. That is because edge states with momenta closer to the Dirac points have larger penetration lengths (compare Fig. 3(b)) and thus explore regions of stronger optomechanical coupling, making their energy momentum-dependent (Fig. 3(d)). In contrast, no transport occurs at the edge of graphene since it supports a flat band of edge modes [30].

The photonic local density of states (LDOS) is experi-

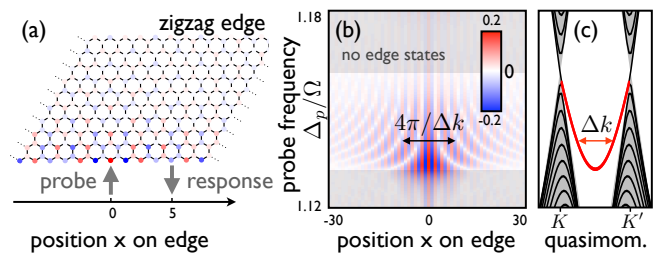


Figure 4: (a) Transport along the edge of a semi-infinite strip. The optical transmission, $t(\omega, x)$ [color code: $\text{Re } t(\omega, x)$] of a locally injected probe laser. (b) Real part of the transmission against the probe detuning ($\Delta_p = \omega_{\text{probe}} - \omega_L$) and the distance x along the edge. See main text for explanation of features. The mechanical transmission is proportional in magnitude to optical one. (c) Close-up of relevant part optomechanical bandstructure. [$g = 0.167\Omega$, other parameters as in Fig. 3 (d)]

mentally accessible via reflection/transmission measurements, e.g. with a tapered fiber probe brought close to the sample. The LDOS on site j , $\rho_j(\omega)$, characterizes the probability to inject a photon with frequency ω . Figure 3(c) shows the LDOS for sites in the bulk (gray) and at the edge (black line). Typical features, like the vanishing DOS at the Dirac points, are smeared out slightly by dissipation. The edge states show up as two peaks. For weak coupling one would naively expect a single edge state peak broadened by dissipation. However, figure 3(e) shows a peak with a narrow dip on top. This can be understood as optomechanically induced transparency [1], an interference effect visible for $\Gamma \ll \kappa$. We note that the gradient in g leads to the formation of additional bands of edge states, cf. close-up in Fig. 3(d).

Edge state transport - The zigzag edge forms a polariton waveguide for excitations injected by a local probe at the edges. Its group velocity is tunable in-situ via the laser amplitude. Although the edge states are not protected by a band gap, the transmission remains mainly along the edge, see Fig. 4(a). Figure 4(b) depicts the optical transmission vs. the propagation distance and the probe frequency. For small probe frequencies there are no edge states, thus the response is local and weak. Increasing the probe frequency makes edge states resonant, leading to transmission along the edge. For a given probe frequency, two edge modes are resonant, with a quasimomentum difference Δk . This explains the interference pattern, with transmission minima at $x = \pm n\pi/\Delta k$. The mechanical transmission mirrors the optical one ($|t_M(\omega, x)| \propto |t_O(\omega, x)|$) for strong coupling, and there is no transport for weak coupling (a flat edge state band).

Optomechanical Klein tunneling - The in-situ tunability of optomechanical metamaterials allows to create arbitrary effective potential landscapes simply by generating a spatially non-uniform driving laser profile. This can

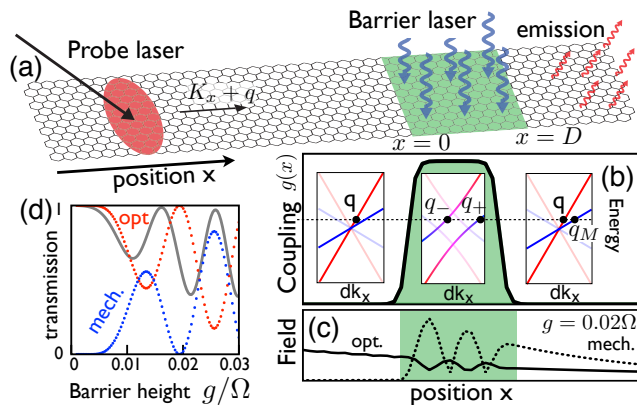


Figure 5: Optomechanical Klein tunneling: (a) A tilted probe laser injects photons at quasimomentum $\mathbf{K} + \mathbf{q}$ that transmit through a barrier (green) as photons and/or phonons without any backscattering. Emitted light (red arrows) can be detected experimentally. (b) Position-dependent profile of the optomechanical coupling $g(x)$, proportional to the light amplitude of the strong drive laser that creates the barrier. Insets: The local spectrum in each region, and the allowed quasimomenta at the probe frequency. (c) Optical and mechanical field ($\langle \hat{a}_j \rangle$ and $\langle \hat{b}_j \rangle$). (d) Optical and mechanical transmission against barrier height. (gray line: optical transmission as predicted analytically from the optomechanical Dirac equation) [Parameters: $\kappa = 0.005\Omega$, $\Gamma = 0.001\Omega$, $J = \Omega/6$, $K = J/10$]

be nicely illustrated in a setup that permits the study of Klein tunneling, the unimpeded transmission of relativistic particles through arbitrary long and high potential barriers. Electrons in graphene realize a special variant of this [36]. Here, we show that the backscattering of Dirac polaritons impinging on an optomechanical barrier is suppressed. Moreover, photons can be converted into phonons (and vice versa) while being transmitted.

To create a barrier for Dirac photons propagating in the array, we make use of the distinctive *in-situ* tunability of optomechanical metamaterials. As shown in Fig. 5(a), when a region of width D is illuminated by a strong control laser (of detuning $\Delta = -\Omega$), a position-dependent optomechanical coupling $g(x)$ is created. This region represents a barrier for Dirac photons injected by a probe laser at another spot. We first solve the scattering problem within the Dirac Hamiltonian (2) in the presence of a barrier with infinitely sharp edges: $g(x) = g$ for $0 < x < D$ and 0 otherwise. We consider a right-moving photon with quasimomentum perpendicular to the barrier, $|\psi_{\text{in}}\rangle = e^{iq_0x}|\sigma_x = 1, \tau_z = 1\rangle$. Backscattering is forbidden, because the helicity is conserved and only the right-moving waves [bold lines in Fig. 5(b)], have positive helicity $\sigma_x = 1$. Thus, the wave is entirely transmitted. Beyond the barrier, it is a superposition of photons and

phonons:

$$|\psi_{\text{out}}\rangle = t_O e^{iq_0x} |1, 1\rangle + \sqrt{v_O/v_M} t_M e^{iq_Mx} |1, -1\rangle, \quad (4)$$

where $q_M = v_O q_0 / v_M$. Note that $|t_M|^2$ can be interpreted as the probability that the photon is converted into a phonon, with $|t_O|^2 = 1 - |t_M|^2$ ensuring conservation of probability. Matching the solutions of the Dirac equation in the different regions, we find

$$|t_M|^2 = \sin^2[(q_+ - q_-)D/2] / [1 + v_O^3 q_0^2 / (4v_M g^2)], \quad (5)$$

where q_{\pm} are the two momenta of the right-moving polaritons in the interacting region, at the probe frequency. In a more accurate description, we compute numerically the stationary light amplitude $\langle \hat{a}_j \rangle$ and the mechanical displacements $\langle \hat{b}_j \rangle$ using the full Hamiltonian (1) and including also dissipation, see Supplemental Information. We assume the probe laser to be injected at a finite distance from the barrier, in a Gaussian intensity profile, see Fig. 5(a). The solution, depicted in Fig. 5(c), shows all the qualitative features predicted using the effective relativistic description of Eq. (5). Inside the barrier, photons are converted back and forth into phonons. Phonons reach higher probabilities, since their speed is smaller ($v_M < v_O$), and their decay length is shorter (for realistic parameters $\Gamma/v_M > \kappa/v_O$). We deliberately chose a steep barrier (on the scale of the lattice constant), to illustrate a small Umklapp backscattering to the other Dirac point (tiny wiggles for $x < 0$). The ratio of the phonon current to the complete current at $x_0 > D$, $v_O |a_0|^2 / (v_M |b_0|^2 + v_O |a_0|^2)$, serves as an estimate for the phonon transmission probability $|r|^2$. Figure 5(d) shows the optical and mechanical transmission against the barrier height, which can be tuned via the control laser. The fact that the numerical results with dissipation differ from the theoretical expectation (grey line: $|t_O|^2$) is mostly due to $v_M \ll v_O$. Having a large mechanical quasimomentum, $q_M = v_O q_0 / v_M \gg q_0$, diminishes slightly the quality of the Dirac approximation.

Experimental realizability - The strong coupling regime, $g > \kappa$, is routinely reached on several optomechanical platforms, including optomechanical crystals. It is also crucial to avoid a phonon-lasing instability, which requires $J \lesssim \Omega/3$ (see Supplemental Information). In principle, J can be made small by design (e.g. distance between sites [19–21]), although disorder effects become more pronounced at smaller J . In $2D$, even for frequency fluctuations of the order of J , the Anderson localization length is several hundred sites, safely exceeding realistic sample sizes. Disorder which is not smooth on the scale of the lattice constant may still induce Umklapp scattering between different Dirac points. Numerical simulations indicate that the Klein tunneling is robust for disorder strengths of 10% of J .

Outlook - Optomechanical metamaterials will offer a highly tunable platform for probing Dirac physics using

tools distinct from other systems. Future studies could investigate the rich nonlinear dynamics expected for blue detuning, which would create novel particle pair creation instabilities for a bosonic massless Dirac system. Pump-probe experiments could reveal time-dependent transport processes. Novel features can also be generated by modifying the laser drive, e.g. optical phase patterns could produce effective magnetic fields and topologically nontrivial band structures [37], and a controlled time-evolution of the laser would allow to study adiabatic changes, sudden quenches and Floquet topological insulators [38].

We acknowledge support via an ERC Starting Grant OPTOMECH, via the DARPA program ORCHID, and via ITN cQOM.

Supplemental material for the article: “Optomechanical Dirac Physics”

M Schmidt¹, V Peano¹ and F Marquardt^{1,2}

¹University of Erlangen-Nürnberg, Staudtstr. 7, Institute for Theoretical Physics, D-91058 Erlangen, Germany

²Max Planck Institute for the Science of Light, Günther-Scharowsky-Straße 1/Bau 24, D-91058 Erlangen, Germany

Classical stationary solutions

In a frame rotating with the driving, the equations of motion for the classical fields (averaged over classical and quantum fluctuations) of an optomechanical array read

$$\begin{aligned}\dot{\beta}_j &= (-i\Omega - \Gamma/2)\beta_j + ig_0|\alpha_j|^2 + i\sum_l K_{jl}\beta_l, \\ \dot{\alpha}_j &= (i\Delta^{(0)} - \kappa/2)\alpha_j + i2g_0\alpha_j\text{Re}\beta_j + i\sum_l J_{jl}\alpha_l + \sqrt{\kappa}\alpha_L.\end{aligned}\quad (\text{S.6})$$

Here, α_L is the laser amplitude and $\Delta^{(0)} = \omega_L - \omega_{\text{cav}}^{(0)}$ is the (bare) detuning. Notice that, in deriving the above equations, we have just incorporated a general coherent coupling \hat{H}_{hop} to the standard equations for single uncoupled optomechanical cells [1]. Implicitly, we have assumed that the dissipation is caused by independent fluctuations on the different lattice sites. For an infinite array one can readily find a stationary solution of the classical equations (S.6) using the mean field ansatz, $\alpha_j = \alpha$ and $\beta_j = \beta$. The resulting equations have the same form as the equations for single-mode optomechanics [39]

$$\alpha = \sqrt{\kappa}\alpha_L/[\Delta^{(0)} + 2g_0\beta - \nu_O + i\kappa/2], \quad \beta = g_0|\alpha|^2/(\Omega + \nu_M). \quad (\text{S.7})$$

As in the standard case, the radiation pressure induced mechanical displacement β translates into a shift of the optical mode eigenfrequencies, $-2g_0\beta$. In the main text, we incorporate this shift in the effective detuning $\Delta = \Delta^{(0)} + 2g_0\beta$. An additional shift of the mechanical and optical eigenfrequencies is induced by the coupling to the neighboring sites, $\nu_O = -\sum_l J_{jl}$ and $\nu_M = -\sum_l K_{jl}$ (for nearest neighbor hopping $\nu_O = 3J$ and $\nu_M = 3K$). For a finite array the stationary fields α_j and β_j are not independent of j . In this case, we solve the classical equations (S.6) numerically.

Linearized Langevin equations

In our work, we apply the standard approach of linearizing the dynamics around the classical solutions [40], the linearized Langevin equations read

$$\begin{aligned}\dot{\hat{b}}_j &= i\hbar^{-1}[\hat{H}', \hat{b}_j] - \Gamma\hat{b}_j/2 + \sqrt{\Gamma}\hat{b}_j^{(\text{in})} = (-i\Omega - \Gamma/2)\hat{b}_j + ig_j\hat{a}_j + ig_j\hat{a}_j^\dagger + i\sum_l K_{jl}\hat{b}_l + \sqrt{\gamma}\hat{b}_j^{(\text{in})}, \\ \dot{\hat{a}}_j &= i\hbar^{-1}[\hat{H}', \hat{a}_j] - \kappa\hat{a}_j/2 + \sqrt{\kappa}\hat{a}_j^{(\text{in})} = (i\Delta_j - \kappa/2)\hat{a}_j + ig_j(\hat{b}_j + \hat{b}_j^\dagger) + i\sum_l J_{jl}\hat{a}_l + \sqrt{\kappa}\hat{a}_j^{(\text{in})}\end{aligned}\quad (\text{S.8})$$

with the noise correlators

$$\begin{aligned}\langle \hat{a}_j^{(\text{in})}(t)\hat{a}_l^{(\text{in})\dagger}(0) \rangle &= \kappa\delta_{jl}\delta(t), & \langle \hat{a}_j^{(\text{in})\dagger}(t)\hat{a}_l^{(\text{in})}(0) \rangle &= 0, \\ \langle \hat{b}_j^{(\text{in})}(t)\hat{b}_l^{(\text{in})\dagger}(0) \rangle &= \Gamma(\bar{n} + 1)\delta_{jl}\delta(t), & \langle \hat{b}_j^{(\text{in})\dagger}(t)\hat{b}_l^{(\text{in})}(0) \rangle &= \Gamma\bar{n}\delta_{jl}\delta(t).\end{aligned}\quad (\text{S.9})$$

The output fields are related to the fields in the array and the input fields by the input output relations [40],

$$\hat{a}_j^{(\text{out})} = \hat{a}_j^{(\text{in})} - \sqrt{\kappa}\hat{a}_j, \quad \hat{b}_j^{(\text{out})} = \hat{b}_j^{(\text{in})} - \sqrt{\Gamma}\hat{b}_j. \quad (\text{S.10})$$

Notice that $\hat{H}' = \hat{H} + \hat{H}_{\text{st}}$ contains also counter rotating terms, $\hat{H}_{\text{st}} = \sum_j g_j (\hat{a}_j^\dagger \hat{b}_j^\dagger + \hat{a}_j \hat{b}_j)$. These terms have been omitted in Eq. (1). This is the standard rotating wave approximation which applies to any side band resolved optomechanical system driven by a red detuned laser with a moderate intensity, $\Omega \gg \kappa$ and $g^2 \lesssim \kappa\Omega$. In an optomechanical array, the laser should be red detuned compared to the lowest frequency optical eigenmode. Thus, in the regime when Dirac photons and Dirac phonons are resonantly coupled ($-\Delta \approx \Omega$), we find the additional constraint $J < \Omega/3$.

Photon emission spectrum

In Fig. 2(d,e), we plot the power spectrum $S(\mathbf{k}, \omega)$ of the photons emitted by the array (periodic boundary conditions have been assumed),

$$S(\mathbf{k}, \omega) \equiv \sum_{\sigma} \int dt \exp[i\omega t] \langle \hat{a}_{\mathbf{k}\sigma}^{\dagger}(t) \hat{a}_{\mathbf{k}\sigma} \rangle. \quad (\text{S.11})$$

Here, $\hat{a}_{\mathbf{k}\sigma}$ are the annihilation operators of the photonic Bloch modes, $\hat{a}_{\mathbf{j}} = (\mathcal{N})^{-1/2} \sum_{\mathbf{r}_j} e^{i\mathbf{k}\cdot\mathbf{r}_j} \hat{a}_{\mathbf{k}\sigma}$ [\mathbf{r}_j is the position counted off from a site on sublattice A and \mathcal{N} is the number of unit cells]. In a large array (where finite size effects are smeared out by dissipation), $S(\mathbf{k}, \omega)$ is proportional to the angle-resolved radiation emitted by the array at frequency $\omega_L - \omega$.

For periodic boundary conditions and nearest neighbor hopping, the Langevin equations (S.8) can be solved analytically (including also the counter rotating terms). By plugging the corresponding solutions into the definition (S.9) and taking into account the correlators Eqs. (S.9), we find

$$S(\mathbf{k}, \omega) = \sum_{\sigma} \frac{4\kappa g^4 \Omega^2 + \Gamma \sigma_M(\omega, \Delta(\mathbf{k}, \sigma), \Omega(\mathbf{k}, \sigma))}{|\mathcal{N}(\omega, \Delta(\mathbf{k}, \sigma), \Omega(\mathbf{k}, \sigma))|^2} \quad (\text{S.12})$$

in terms of the analytical functions

$$\begin{aligned} \sigma_M(\omega, \Delta, \Omega) &= g^2 |\chi_O(\omega, \Delta)|^{-2} [(\bar{n} + 1) |\chi_M(-\omega, \Omega)|^{-2} + \bar{n} |\chi_M(\omega, \Omega)|^{-2}] \\ \mathcal{N}(\omega, \Delta, \Omega) &= [\chi_O(\omega, \Delta) \chi_M(\omega, \Omega) \chi_O^*(-\omega, \Delta) \chi_M^*(-\omega, \Omega)]^{-1} + 4g^2 \Delta \Omega. \end{aligned}$$

Here, we have introduced the free susceptibilities $\chi_O(\omega, \Delta) = [\kappa/2 - i(\omega + \Delta)]^{-1}$ and $\chi_M(\omega, \Omega) = [\Gamma/2 - i(\omega - \Omega)]^{-1}$. Moreover, $-\Delta(\mathbf{k}, \sigma)$ and $\Omega(\mathbf{k}, \sigma)$ are the spectra of tight-binding photons and phonons on the honeycomb lattice (the photon spectrum is defined in the rotating frame), respectively. They are given by $\Delta(\mathbf{k}, \sigma) = \Delta + Jf(\mathbf{k}, \sigma)$ and $\Omega(\mathbf{k}, \sigma) = \Omega - Kf(\mathbf{k}, \sigma)$ where $f(\mathbf{k}, \sigma) = \pm |1 + e^{i\mathbf{k}\cdot\mathbf{a}_1} + e^{i\mathbf{k}\cdot\mathbf{a}_2}|$.

Local Density of states and transmission amplitudes

In Fig. 3 and 4 of the main text, we plot the local photonic densities of states (LDOS) on site \mathbf{j} , $\rho(\omega, \mathbf{j})$ and the transmission amplitude $t_O(\omega, \mathbf{l}, \mathbf{j})$ relating the emission in the output field at site \mathbf{l} to an input probe field at sites \mathbf{j} with frequency ω , $\langle \hat{a}_{\mathbf{l}}^{\text{(out)}}(t) \rangle = t_O(\omega, \mathbf{l}, \mathbf{j}) \langle \hat{a}_{\mathbf{j}}^{\text{(in)}}(t) \rangle$ where $\langle \hat{a}_{\mathbf{j}}^{\text{(in)}}(t) \rangle = f e^{-i\omega t}$. These two quantities are directly related to the photonic retarded Green's function

$$\tilde{G}_{OO}(\omega, \mathbf{j}, \mathbf{l}) = -i \int_{-\infty}^{\infty} dt e^{i\omega t} \Theta(t) \langle [\hat{a}_{\mathbf{j}}(t), \hat{a}_{\mathbf{l}}^{\dagger}(0)] \rangle.$$

In fact, the density of state is defined as

$$\rho(\omega, \mathbf{j}) = -2\text{Im} \tilde{G}_{OO}(\omega, \mathbf{j}, \mathbf{j}) \quad (\text{S.13})$$

where $\tilde{G}_{OO}(\omega, \mathbf{j}, \mathbf{l}) = -i \int_{-\infty}^{\infty} dt e^{i\omega t} \Theta(t) \langle [\hat{a}_{\mathbf{j}}(t), \hat{a}_{\mathbf{l}}^{\dagger}(0)] \rangle$. Moreover, using Kubo formula and the input output relation Eq. (S.10), we find the photon transmission amplitude to be

$$t_O(\omega, \mathbf{l}, \mathbf{j}) = \delta_{\mathbf{l}\mathbf{j}} - i\kappa \tilde{G}_{OO}(\omega, \mathbf{l}, \mathbf{j}). \quad (\text{S.14})$$

For an infinite strip of width M unit cells, it is most convenient to introduce the partial Fourier transform of $\tilde{G}(\omega, \mathbf{j}, \mathbf{l})$,

$$\tilde{G}_{OO}(\omega, \mathbf{j}, \mathbf{l}) = N^{-1} \sum_k e^{i(n_j - n_l)k_x} \tilde{G}_{OO}(\omega, k_x; m_j, \sigma_j; m_l, \sigma_l). \quad (\text{S.15})$$

Here, k_x is the momentum in the translationally invariant direction (x -axis). Formally, we have introduced a finite length of N cells and periodic boundary conditions. However, the spurious finite size effects induced by this assumption are smeared out by dissipation for an appropriately large N . After taking the partial Fourier transform of the classical

displaced fields $\langle \hat{a}_i \rangle$ and $\langle \hat{b}_j \rangle$, we organize their Fourier components $\alpha_{k_x m \sigma}, \beta_{k_x m \sigma}$ in a $2M$ -dimensional vector \mathbf{c}_k with equation of motion in the form $i\langle \dot{\mathbf{c}}_k \rangle = A_k \langle \mathbf{c}_k \rangle$ (when no probe laser is present). The $2M \times 2M$ matrix A_k is obtained from the Langevin equations (S.8) by neglecting the counter rotating terms. Thus, the Green's function $\tilde{G}_{OO}(\omega, k_x; m_j, \sigma_j; m_l, \sigma_l)$ is the block of the matrix $\tilde{G}(\omega, k) = (\omega - A_k)^{-1}$ which acts on the optical subspace of $\hat{\mathbf{c}}_k$. The LDOS and transmission amplitudes $t(\omega, \mathbf{i}, \mathbf{j})$ are then readily calculated from Eqs. (S.13-S.15)

Details of the numerical calculation of the Klein tunneling of photons and phonons

In Fig. 5, we consider an infinite strip with armchair edges and a width of $N = 500$ unit cells (in the x -direction). Notice that the unit cell of an armchair strip is formed by four sites. Thus, the photon and phonon dynamics is described by the Langevin equations (S.8) with the multi-index $\mathbf{j} = [m_x, m_y, s]$, where $m_x = 0, \dots, N$, $m_y \in Z$, and $s = 1, 2, 3, 4$. The optomechanical barrier created by the strong control laser is translationally invariant in the y -direction, $g(m_x) = g[e^{\beta(m_x - m_R)} + 1]^{-1} [e^{\beta(m_L - m_x)} + 1]^{-1}$ with $\beta = 2$, $m_L = 200$, and $m_R = 213$. The probe laser has a gaussian intensity profile in the x -direction with average inplane momentum close to the \mathbf{K} symmetry point, $\hat{a}_{\mathbf{j}}^{(\text{in})} = \exp[-i\Delta_p t - (m_x - m_0)^2 / \delta m^2 + i\mathbf{r}_{\mathbf{j}} \cdot \bar{\mathbf{k}}]$. We choose $\bar{\mathbf{k}} - \mathbf{K} = (0.029/a, 0)$, $\Delta_p = \Omega + v_O |\bar{\mathbf{k}} - \mathbf{K}|$, $m_0 = 90$, and $\delta m = 30$. The other parameters are given in the main text. The stationary Langevin equations have been solved by computing numerically the Green's functions for $k_y = 0$.

-
- [1] Markus Aspelmeyer, Tobias J. Kippenberg, and Florian Marquardt. Cavity optomechanics. *ArXiv*, page 1303.0733, (to be published in Rev. Mod. Phys. 2014).
 - [2] Mian Zhang, Gustavo S. Wiederhecker, Sasikanth Manipatruni, Arthur Barnard, Paul McEuen, and Michal Lipson. Synchronization of micromechanical oscillators using light. *Phys. Rev. Lett.*, 109:233906, 2012.
 - [3] Mahmood Bagheri, Menno Poot, Linran Fan, Florian Marquardt, and Hong X. Tang. Photonic cavity synchronization of nanomechanical oscillators. *Phys. Rev. Lett.*, 111:213902, 2013.
 - [4] Jeff T. Hill, Amir H. Safavi-Naeini, Jasper Chan, and Oskar Painter. Coherent optical wavelength conversion via cavity-optomechanics. *Nat. Commun.*, 3:1196, 2012.
 - [5] Chunhua Dong, Victor Fiore, Mark C. Kuzzyk, and Hailin Wang. Optomechanical dark mode. *Science*, 338(6114):1609–1613, 2012.
 - [6] Ivan S. Grudinin, Hansuek Lee, O. Painter, and Kerry J. Vahala. Phonon laser action in a tunable two-level system. *Phys. Rev. Lett.*, 104:083901, 2010.
 - [7] Gaurav Bahl, Matthew Tomes, Florian Marquardt, and Tal Carmon. Observation of spontaneous brillouin cooling. *Nature Phys.*, 8(3):203–207, 2012.
 - [8] Lu Ding, Christophe Baker, Pascale Senellart, Aristide Lemaitre, Sara Ducci, Giuseppe Leo, and Ivan Favero. High frequency gas nano-optomechanical disk resonator. *Phys. Rev. Lett.*, 105:263903, 2010.
 - [9] Andrea M. Armani, Akil Srinivasan, and Kerry J. Vahala. Soft lithographic fabrication of high q polymer microcavity arrays. *Nano Lett.*, 7(6):1823–1826, 2007.
 - [10] E. Verhagen, S. Deléglise, S. Weis, A. Schliesser, and T. J. Kippenberg. Quantum-coherent coupling of a mechanical oscillator to an optical cavity modes. *Nature*, 482:63–67, 2012.
 - [11] Andrew A. Houck, Hakan E. Tureci, and Jens Koch. On-chip quantum simulation with superconducting circuits. *Nature Phys.*, 8(4):292–299, 2012.
 - [12] C. A. Regal, J. D. Teufel, and K. W. Lehnert. Measuring nanomechanical motion with a microwave cavity interferometer. *Nature Phys.*, 4(7):555–560, 2008.
 - [13] J. D. Teufel, T. Donner, Dali Li, J. W. Harlow, M. S. Allman, K. Cicak, A. J. Sirois, J. D. Whittaker, K. W. Lehnert, and R. W. Simmonds. Sideband cooling of micromechanical motion to the quantum ground state. *Nature*, 475:359–363, 2011.
 - [14] Matt Eichenfield, Jasper Chan, Ryan M. Camacho, Kerry J. Vahala, and Oskar Painter. Optomechanical crystals. *Nature*, 462(7269):78–82, 2009.
 - [15] Amir H. Safavi-Naeini, Thiago P. Mayer Alegre, Martin Winger, and Oskar Painter. Optomechanics in an ultrahigh-q two-dimensional photonic crystal cavity. *Appl. Phys. Lett.*, 97(18):181106, 2010.
 - [16] E. Gavartin, R. Braive, I. Sagnes, O. Arcizet, A. Beveratos, T. J. Kippenberg, and I. Robert-Philip. Optomechanical coupling in a two-dimensional photonic crystal defect cavity. *Phys. Rev. Lett.*, 106:203902, 2011.
 - [17] Jasper Chan, T. P. Mayer Alegre, Amir H. Safavi-Naeini, Jeff T. Hill, Alex Krause, Simon Groblacher, Markus Aspelmeyer, and Oskar Painter. Laser cooling of a nanomechanical oscillator into its quantum ground state. *Nature*, 478(7367):89–92, 2011.
 - [18] Amir H. Safavi-Naeini, Jeff T. Hill, Seán Meenehan, Jasper Chan, Simon Gröblacher, and Oskar Painter. Two-dimensional phononic-photonic band gap optomechanical crystal cavity. *Phys. Rev. Lett.*, 112:153603, 2014.
 - [19] Amir H Safavi-Naeini and Oskar Painter. Proposal for an optomechanical traveling wave phonon-photon translator. *New J. Phys.*, 13(1):013017, 2011.

- [20] Georg Heinrich, Max Ludwig, Jiang Qian, Björn Kubala, and Florian Marquardt. Collective dynamics in optomechanical arrays. *Phys. Rev. Lett.*, 107:043603, 2011.
- [21] Max Ludwig and Florian Marquardt. Quantum many-body dynamics in optomechanical arrays. *Phys. Rev. Lett.*, 111:073603, 2013.
- [22] D E Chang, A H Safavi-Naeini, M Hafezi, and O Painter. Slowing and stopping light using an optomechanical crystal array. *New J. Phys.*, 13(2):023003, 2011.
- [23] C. A. Holmes, C. P. Meaney, and G. J. Milburn. Synchronization of many nanomechanical resonators coupled via a common cavity field. *Phys. Rev. E*, 85:066203, 2012.
- [24] Michael Schmidt, Max Ludwig, and Florian Marquardt. Optomechanical circuits for nanomechanical continuous variable quantum state processing. *New J. Phys.*, 14(12):125005, 2012.
- [25] M. Bhattacharya and P. Meystre. Multiple membrane cavity optomechanics. *Phys. Rev. A*, 78(4):041801, 2008.
- [26] A. Tomadin, S. Diehl, M. D. Lukin, P. Rabl, and P. Zoller. Reservoir engineering and dynamical phase transitions in optomechanical arrays. *Phys. Rev. A*, 86:033821, 2012.
- [27] André Xuereb, Claudiu Genes, and Aurélien Dantan. Strong coupling and long-range collective interactions in optomechanical arrays. *Phys. Rev. Lett.*, 109:223601, 2012.
- [28] Uzma Akram, William Munro, Kae Nemoto, and G. J. Milburn. Photon-phonon entanglement in coupled optomechanical arrays. *Phys. Rev. A*, 86:042306, 2012.
- [29] Wei Chen and Aashish A. Clerk. Photon propagation in a one-dimensional optomechanical lattice. *Phys. Rev. A*, 89:033854, 2014.
- [30] A. H. Castro Neto, F. Guinea, N. M. R. Peres, K. S. Novoselov, and A. K. Geim. The electronic properties of graphene. *Rev. Mod. Phys.*, 81:109–162, 2009.
- [31] Or Peleg, Guy Bartal, Barak Freedman, Ofer Manela, Mordechai Segev, and Demetrios N. Christodoulides. Conical diffraction and gap solitons in honeycomb photonic lattices. *Phys. Rev. Lett.*, 98:103901, Mar 2007.
- [32] Marco Polini, Francisco Guinea, Maciej Lewenstein, Hari C. Manoharan, and Vittorio Pellegrini. Artificial honeycomb lattices for electrons, atoms and photons. *Nature Nanotechnology*, 8(9):625–633, 2013.
- [33] T. Jacqmin, I. Carusotto, I. Sagnes, M. Abbarchi, D. D. Solnyshkov, G. Malpuech, E. Galopin, A. Lemaitre, J. Bloch, and A. Amo. Direct observation of dirac cones and a flatband in a honeycomb lattice for polaritons. *Phys. Rev. Lett.*, 112:116402, 2014.
- [34] Amir H. Safavi-Naeini and Oskar Painter. Design of optomechanical cavities and waveguides on a simultaneous bandgap phononic-photonic crystal slab. *Opt. Express*, 18(14):14926–14943, 2010.
- [35] M. Z. Hasan and C. L. Kane. Colloquium: Topological insulators. *Rev. Mod. Phys.*, 82:3045–3067, 2010.
- [36] Andrea F. Young and Philip Kim. Quantum interference and klein tunnelling in graphene heterojunctions. *Nature Phys.*, 5(3):222–226, 2009.
- [37] V. Peano, C. Brendel, M. Schmidt, and F. Marquardt. Topological phases of sound and light. *ArXiv*, page 1409.5375, 2014.
- [38] Takashi Oka and Hideo Aoki. Photovoltaic hall effect in graphene. *Phys. Rev. B*, 79:081406, 2009.
- [39] P. Meystre, E. M. Wright, J. D. McCullen, and E. Vignes. Theory of radiation-pressure-driven interferometers. *J. Opt. Soc. Am. B*, 2(11):1830–1840, Nov 1985.
- [40] D. F. Walls and G. J. Milburn. *Quantum Optics*. Springer, 2008.